

Evolution of Spectral States of Aql X-1 during the 2000 Outburst

Dipankar Maitra and Charles D. Bailyn

Yale University, Department of Astronomy, P.O.Box 208101, New Haven, CT, 06520-8101

`maitra,bailyn@astro.yale.edu`

ABSTRACT

We present the results of detailed analysis of X-ray data in 3-20 keV range from a ~ 70 day outburst of the neutron star transient Aquila X-1 during September-November 2000. Optical monitoring with the YALO 1m telescope was used to trigger X-ray observations with *Rossi X-ray Timing Explorer* (RXTE) in order to follow the outburst from a very early stage. In this paper we discuss the correlated evolution in time of features in the spectral and temporal domains, for the entire outburst. The state transition from low/hard state to high/soft state during the rise of the outburst occurs at higher luminosity than the transition back to low/hard state during the decay, as has also been observed in other outbursts. Fourier power spectra at low frequencies show a broken power law continuum during the rising phase, with the break frequency increasing with time. During the decline from maximum the source evolves to a position in the hardness-intensity plane as well as in the color-color diagram which is similar to, but distinct from, the canonical high/soft state. High frequency quasi-periodic oscillations from 636-870 Hz were seen only during this transitional state.

Subject headings: accretion, accretion disks — stars: neutron — X-rays: binaries — individual (Aquila X-1)

1. Introduction

Soft X-ray transients (SXTs) are an important class of low-mass X-ray binaries (LMXBs). A characteristic property of SXTs is that their luminosity is generally below the detection limit of most X-ray telescopes. However occasionally they brighten up by several orders of magnitude at all wavelengths. Usually X-ray radiation during the low luminosity, low \dot{M} state shows a powerlaw spectrum, suggesting a nonthermal origin of the radiation. For SXTs with a neutron star (NS) as the accretor, sometimes a soft thermal blackbody component can also be seen which is attributed to surface emission from the NS (Campana & Stella 2000;

Rutledge et al. 1999, 2000). The origin of the powerlaw is generally attributed to softer photons that have been upscattered by their interaction with hot electrons in a Comptonizing corona (e.g. Sunyaev & Titarchuk (1980); Nowak (1995, 2002); however see Markoff et al. (2001) who suggest that the powerlaw photons are due to synchrotron emission from jets). The spectra at higher luminosities and hence at higher \dot{M} , however, are largely thermal and can be well fit by assuming a disk shaped blackbody with a variable radial temperature profile given by $T \sim R^{-3/4}$ (Shakura & Sunyaev 1973; Mitsuda et al. 1984). The dominance of hard powerlaw photons in the low luminosity state gives it the name *low/hard* (LH) state, whereas dominance of soft thermal photons in the high luminosity state gives it the name *high/soft* (HS) state. The LH and HS states are the two canonical spectral states of most SXTs. There are a host of other spectral states observed which are various combinations of the powerlaw and thermal spectra, differing in their relative strengths as well as spectral shape (e.g. change in powerlaw photon index Γ). While \dot{M} is likely one of the factors causing spectral state transitions, recent work (Homan et al. 2001; Smith, Heindl, & Swank 2002; Maccarone & Coppi 2003) suggests the existence of factor(s) other than \dot{M} . Thus we are faced with a second parameter problem in explaining the spectra of SXTs and other X-ray binaries.

Aql X-1 has the shortest recurrence time of any SXT known so far, which makes it an excellent system to study. Aql X-1 has been observed to go into outburst approximately once every year, but the periodicity is not fixed (Šimon 2002). Type I X-ray bursts from Aql X-1 (Koyama et al. 1981; Czerny, Czerny, & Grindlay 1987) suggests that the compact object is a weakly magnetized neutron star. The companion is a Roche lobe filling late K star (Chevalier et al. 1999; Welsh et al. 2000) and the system has an orbital period of 18.95 hrs (Welsh et al. 2000), at a distance of 4-6.5 kpc (Rutledge et al. 2001). Based on its evolution on the color-color plane (Hasinger & van der Klis 1989), and its spectral and temporal properties, Aql X-1 has been classified as an ‘atoll’ source (Reig et al. 2000).

In September 2000, Aql X-1 initiated a new outburst. We obtained PCA data triggered by optical observations. The RXTE data for this outburst have been analyzed by Yu et al. (2003), who reported hard X-ray flares preceding the transition to the soft state and 1-20 Hz QPO in the outburst rise. From the similarity in spectral/temporal behaviour between this outburst of Aql X-1 and other black hole transients, Yu et al. (2003) suggest a similar origin for QPOs and the continuum shape of PDS for both neutron star transients as well as black hole transients.

Here we present our results of spectral and temporal analysis of the data obtained during the 2000 outburst of Aql X-1. We find that initially the spectrum was dominated by hard powerlaw photons with $\Gamma < 2$, with little or no disk. As the source luminosity increased, the

source made a very rapid transition from LH state to a HS state, dominated by the disk and also a steep ($\Gamma > 3$) falling powerlaw. However, during the decaying phase, the transition back to LH state occurred at a lower luminosity (and hence lower inferred mass accretion rate) than the transition from LH to HS state. This phenomenon has been observed for other outbursts of Aql X-1, as well as other SXTs (Miyamoto et al. (1995); Maccarone & Coppi (2003) and references therein). Thus the source traces a hysteresis loop in the X-ray hardness-intensity diagram. We also find that, during the final stages of the HS state the source becomes softer in color and occupies a new region in the color-color plane. The hysteresis loop, as well as presence of this ‘transitional soft state’(TSS) are hard to explain in the regime of standard single flow accretion models.

In §2 we describe our observations and data analysis techniques. The results of broad-band spectral color analysis is described in §2.1. A detailed spectral deconvolution is presented in §2.2. The temporal regime between 0.1Hz - 4kHz is analyzed in §2.3, with emphasis on the continuum structure of the low frequency power (§2.3.1) and search for high frequency quasi-periodic oscillations (§2.3.2). In §3 we describe the transitional state during decline associated with the hysteresis loop. Section 4 summarizes our results and speculates on possible physical mechanisms that might be causing the observed spectral and temporal features and their evolution.

2. Observations and Data Analysis

The quiescent flux from Aql X-1 is too low for the *All Sky Monitor* (ASM) (Levine et al. 1996) on the Rossi X-ray Timing Explorer satellite (RXTE) (Bradt, Rothschild, & Swank 1993) to detect. Even during the rising phase of the outburst, by the time the ASM starts seeing counts, the source is already quite bright in the Proportional Counter Array (PCA)(Jahoda et al. 1996). However, from previous observations it has been observed that the optical flux for Aql X-1 and other SXTs rises several days before the X-ray (Orosz et al. 1997; Jain 2001). Therefore ground based optical monitoring using the Yale 1m telescope at CTIO, Chile, operated by the YALO consortium (Bailyn et al. 1999) was used to trigger the series of target-of-opportunity (TOO) X-ray observations. The additional lead time provided by our daily optical monitoring program allowed us to observe the source from the very early phase of the outburst. Observations continued until the source again faded below detection limit about two months later.

The data presented in this paper were collected with the PCA instrument on RXTE. Our observations of Aql X-1 started from 24th September 2000 (MJD 51811.3). We observed until the end of November 2000 when it again faded below RXTE’s detection limit. The

source was observed for a total of about 355 ks divided in 63 pointed PCA observations. The times reported in this work are represented as offsets from MJD 51800. In Fig. 1 the distribution of observing time is shown on top panel and the background subtracted PCA (\approx 2-60 keV) lightcurve at the bottom. The first four columns of Table 1 gives the serial number of the observation, observation IDs, observation start time in MJD and exposure times in kiloseconds. Our first observation is at MJD \sim 51814 days. Observations were conducted typically once a day. Between MJD \sim 51820 days and 51822 days, the total count-rate jumped from \sim 475 counts/sec/pcu to \sim 1175 counts/sec/pcu. This sudden jump was accompanied by a sharp change from “low-hard” spectral state to “high-soft” state (discussed in detail later). However lack of data in-between prevented us from observing details of the transition from hard to soft state. The declining phase of the outburst however was much slower and the spectral state transitions are better resolved during the declining phase.

The *Standard 2* PCA data for the observations were extracted using the FTOOLS 5.0.2 package. Since the count-rates are small during the beginning and end of the outburst, we have used data from the observations when the maximum number PCUs were turned on. In order to avoid looking at the earth, we considered data only when the elevation angle was 10° or more. Any data with (i) offset pointing more than $0^\circ.02$; or (ii) within 30 mins of SAA passage; or (iii) trapped electron contamination more than the prescribed value (i.e $ELECTRON2 > 0.1$) were rejected. Appropriate faint/bright background models were used when the source was fainter/brighter than 40 counts/s/PCU.

2.1. Fluxes and Colors

Following Gierliński & Done (2002), we extracted *standard 2* lightcurves for four energy bands, viz. 3-4, 4-6.4, 6.4-9.7 and 9.7-16 keV (corresponding to binned Std2 channels 5-6, 7-11, 13-19 and 20-33 respectively). Two bursts were detected during the rising phase and were excluded from analysis (Yu et al. 2003). The hardness-ratio for each observation was calculated from the ratio of counts in the hardest band (9.7-16 keV) to the softest band (3-4 keV; see Fig. 2). For typical spectral fits the softest band (3-4 keV) contains mostly thermal photons whereas the hardest band (9.7-1.6 keV) is dominated by powerlaw photons. Hence the (9.7-16 keV)/(3-4 keV) hardness ratio is an indicator of the ratio of powerlaw photons to the disk photons. As expected, the spectra remain hard during the low state, but make a very rapid transition to the soft state between MJD \sim 51820 and 51822. The source remains soft until MJD \sim 51864 after which we see a smooth transition to the hard state. However the transition back to the LH state from the HS state during the decaying phase occurs more slowly. However it is to be noted that since we only consider photons

within certain energy-bands, the numerical values of the hardness-ratios do not say much about the physical processes nor is the hardness ratio equal to disk/powerlaw luminosity.

As seen in Fig. 3, the source traces a hysteresis loop over the entire outburst cycle in the hardness-luminosity plane [(9.7-16)keV/(3-4)keV hardness-ratio vs. (6.4-9.7)keV count-rate]. Aql X-1 and few other SXT’s are now known to show this feature (Maccarone & Coppi 2003; Munoz et al. 2002; Reig et al. 2000; Cui et al. 1998). The transition from hard-to-soft state takes place at a (6.4-9.7 keV) luminosity ~ 10 times higher than the luminosity at which it returns back to the hard state. The observed trend in evolution is very similar to what was observed by Maccarone & Coppi (2003) using ASM data during the 1998 outburst.

A particularly interesting feature of the spectral evolution emerges when one considers the evolution in the color-color diagram. Soft color was defined as a ratio of 4-6.4 to 3-4 keV count rates, and hard color as a 9.7-16 over 6.4-9.7 keV ratio. We plotted each observation (dwell) as one point on the color-color diagram. Since the evolution of the source on the color-color plane during an observation is small compared to the entire space it spans during the entire outburst cycle, this is a reasonable procedure to track the time evolution during the entire outburst (Fig. 4, top panel). We find that the overall soft state (hard color ≤ 0.4) has two sub-states. Once the source makes a transition from hard state to the soft state, it occupies the lower right of the CC diagram (shown by open circles in the bottom panel of Fig. 4) and stays there as long as the luminosity is close to that of peak outburst (plateau in Fig. 1). Once the decay starts appreciably, the source moves slightly to the left in CC plane (filled circles in Fig. 4), corresponding to the TSS, and stays there until it makes another sharp transition to the initial hard state. The HS state and the TS state occupy disjoint (though neighboring) regimes of the color-color diagram.

2.2. Spectral deconvolution

Spectral analysis was carried out with the XSPEC software (v.11.0.1). We used the PCA *Standard 2* data in the energy range of 3-20 keV where PCA calibrations are the best. The spectral model we adopted consists of two additive components: a multi-colored disk (MCD) or disk blackbody (DBB) (Mitsuda et al. 1984), plus a powerlaw. Galactic X-ray absorption was accounted for using the multiplicative photoelectric absorption model *wabs* (Morrison & McCammon 1983), with a constant hydrogen column density of 3.4×10^{21} atoms/cm², the galactic value along the line of sight towards Aql X-1. It was found that the inclusion of another multiplicative component, a smeared edge (*smedge* in XSPEC terminology) greatly improved the spectral fits. The threshold energy of the edge was constrained to lie between 7-8 keV. Assuming a systematic error of 1% for all PCA channels (Homan et al. 2001;

Maccarone & Coppi 2003), the above model gave good fits with χ^2/dof close to 1. Including an Iron line near 6.5 keV improved the fits only marginally and hence we have omitted the feature.

The results of the fits are tabulated in Table 1 and plotted in Fig. 5. As expected, both the disk and powerlaw normalizations rise/fall during the rise/decay of the outburst. In the hard state, the powerlaw photon index Γ is flatter (< 2) compared to its value in the soft state when it is always steeper than 2. Remarkably, all but the disk normalization remains very constant throughout the soft state. The only change when the source moves from the HS to the TSS is that the disk normalization falls as shown in Fig. 6.

2.3. Temporal Analysis

We performed a Leahy-Normalized fast Fourier transform (Leahy et al. 1983) for every 64s segment using *Event* mode data of each observation for the full PCA (\sim 2-60 keV) energy band. The *powspec* tool in XRONOS package was used to calculate the power density spectrum (PDS). The data was binned into 2^{-6} s time bins, corresponding to a Nyquist frequency of 32 Hz. The error bars in the average power spectrum were calculated by evaluating the standard deviation of the average power for each frequency. These individual PDSs were then added to obtain average power-density spectrum for each dwell. The PDS were rebinned logarithmically to increase S/N. Finally white Poisson noise was subtracted and the PDS renormalized by the mean count rate, as discussed by van der Klis (1995). Thus the final PDS has the units of $(\text{rms}/\text{mean})^2 \text{ Hz}^{-1}$. The total time variability in a certain frequency range was estimated by fitting the corresponding PDS with a power-law or a combination of power-law and Lorentzian, and integrating over the frequency range. Most of the power comes from frequencies less than 30 Hz, beyond which the spectra is essentially dominated by white Poisson noise.

2.3.1. Low Frequency Power

During the LH rising phase, the power spectra in the range of 0.1-30 Hz exhibit a shallow powerlaw continuum up to a break frequency f_{br} . Beyond the break frequency the noise falls as f^{-1} . To describe the continuum behavior we fitted a broken power law model of the form:

$$\text{PDS}(f) = \begin{cases} C \left(\frac{f}{f_{br}} \right)^{\alpha_1}, & f < f_{br} \\ C \left(\frac{f}{f_{br}} \right)^{\alpha_2}, & f \geq f_{br} \end{cases}$$

where α_1 and α_2 are power law indices, and f_{br} is defined above. The constant C is chosen so that the integral of the continuum model gives the correct power, expressed as fractional rms variability.

Broad QPO-like humps were also observed in some of the spectra (see Fig. 7). With the progress of the outburst the break frequency as well as the QPO frequency appears to increase (Yu et al. 2003) whereas the total continuum power level decreases. This trend was also observed during the 1999 outburst of the same source (Jain 2001) and for Cyg X-1 (Belloni & Hasinger 1990; Belloni et al. 2002). Table 2 lists the break frequency, powerlaw indices and the relevant QPO parameters for these dwells, averaged over the exposure times in each dwells.

The soft state power spectrum is relatively featureless, the rms amplitudes are small and can be modelled by a flat powerlaw at frequencies lower than ~ 10 Hz, and dominated by Poisson noise residuals at higher frequencies. Occasionally the signature of a break or a hump is observed, but the errors are too large to identify any feature conclusively, or to trace the evolution of any feature.

The variation of total power within 0.1-30 Hz frequency range (expressed in percentage rms variability), over the entire outburst is shown in Fig. 8. The strong correlation of the rms variability with spectral hardness (Fig. 2) strongly suggests that most of the time variability indeed comes from the hard, nonthermal photons presumably Compton upscattered in the corona above the accretion disk. The rms energy spectra for a particular dwell (Fig. 9) also supports the argument that most of the time variability comes from hard photons.

2.3.2. kHz QPOs

We also performed a Leahy-Normalized fast Fourier transform for every 128s segment of the *Event* data sets, extending up to 4 kHz in frequency. The frames were weighted and co-added to obtain average power-density spectrum for each observation. We found nine kilohertz QPOs in various segments of our 41st and 47th-51st observations. All the QPOs were observed during the decaying phase of the outburst, when the source was in the TSS. Near the kHz QPOs, the continuum is essentially flat with variations solely due to Poisson fluctuation in the data. The QPO profile is modelled by a simple Lorentzian of the form

$$PDS(f) = \frac{(rms_{qpo})^2}{\pi} \frac{\Delta f/2}{(f - f_{qpo})^2 + (\Delta f/2)^2}$$

where rms_{qpo} is the integrated fractional rms amplitude of the QPO, f_{qpo} is the center of the Lorentzian and Δf is its full width at half maximum (FWHM)(Cui et al. 1997, 1998;

Zhang et al. 1998). Best fit estimates for the observed QPOs are given in Table 3. In Fig. 10 we show a sample time-averaged PDS from 0.01 Hz to 4 kHz for the dwell starting MJD 51864.17. There is no observable change in the powerspectrum or QPO frequency during the dwell. The last QPO occurs just before the source makes the transition back to hard state from the soft state. We searched the frequency regime up to 4kHz but there were no evidence of any other harmonics.

Previous work on kHz QPOs has shown an interesting correlation between source luminosity and QPO frequency (van der Klis 2001; Kaaret et al. 1998). It is observed that on a smaller timescale of hours (e.g. within a single observation dwell), QPO frequency is well correlated with the flux. However this correlation is lost in larger timescales of days (e.g between observations). This leads to formation of “parallel tracks” in $\nu_{QPO} - Flux$ plane. This has been related to existence of two accretion flows rather than one. Owing to comparatively large number of kHz QPOs observed during the 2000 outburst of Aql X-1 and relatively high photon count rate, we could carry out FFT of the data for every 128s segment and track the QPO evolution (Fig 11). We find that at lower count rates the tracks are somewhat more correlated and show the “parallel tracks” more clearly. At higher count-rates, however, even the short-term correlation seems to break down. This is in agreement with the observations of kHz QPOs in 4U 1608-52 by Méndez et al. (1999) (see their Fig.2).

3. The Transitional Soft State

As seen in §2.1.2 and Fig. 3, once the source goes into the soft state, it stays in the bottom right corner of the color-luminosity diagram (shown by the filled triangles). It stays in this bottom right corner while the X-ray luminosity remains close to the peak outburst value. In the color-color diagram also the soft state stands out as a separate region, occupying the right side of Fig. 4. We associate this state with the canonical soft state of Aql X-1.

However, as the luminosity decreases from the peak luminosity (the region labelled as “Trans Soft” in Fig. 5), the source still stayed in the soft state for about ~ 10 days before going back to the hard state, thereby tracing the hysteresis loop. During this time when the total source luminosity was below that of the state transition during the rise the source displayed small but consistent differences from the canonical soft state. Thus as the source traces the hysteresis loop, it appears to enter a different state (or substate) that has no counterpart during the rising phase. All the kHz QPOs were observed when the source was in this transitional soft state only.

In the color-color plane, the data taken during the decline (but still in overall soft state)

also occupies a region significantly different from the others. When the source is in the canonical soft state, the soft color has a value > 1.87 , whereas it is softer than this value during the transitional soft state. In contrast, the hard color remains at almost similar values during both substates of the soft state. In the spectral deconvolution (Fig. 5), the signature of this new state is observed in the decrease of disk normalization. Paradoxically, the decrease in the disk flux results in a softer spectrum in the RXTE band passes, since the powerlaw, which does not change, contributes a larger fraction of the flux in the soft band than the medium bands (see Fig. 6). All other spectral parameters viz. the spectral shapes of the disk and powerlaw as well as the powerlaw strength, remain the same over both the HS and TSS.

We suggest that this “transitional soft state” should be considered separately from the canonical soft state. The presence of this state during decline, but not during the rise, provides additional evidence for the existence of a second parameter, a physical parameter other than \dot{M} , that governs state transition in STXs.

4. Discussion

In the context of two flow models of accretion discussed by Smith, Heindl, & Swank (2002, hereafter SHS), accretion can take place either via the accretion disk or through a hot sub-Keplerian halo. The disk photons are soft and have a thermal origin whereas the halo photons comprise the hard powerlaw photons. Any change in the disk mass accretion rate occurs only on viscous timescales which are much longer than the almost free-fall timescales in the halo. Close to peak outburst luminosities, the disk photons dominate the spectrum and according to SHS one should see the *static* soft state. A *dynamic* soft state is seen when the overall mass inflow rate starts decreasing, to which the halo responds much faster than the disk and hence drains out its contents thereby making the spectrum softer. If the two soft states that we observed are indeed the static and dynamic soft states proposed by SHS, then the ~ 10 day decay of Aql X-1 in the dynamic soft state is a direct measurement of viscous timescale of the accretion disk. However, the spectral fits to the data show that the softening in soft color [(4-6.4)keV/(3-4)keV countrates] during the transitional soft state is in fact due to a decrease of flux in the disk, not in the powerlaw. This is contrary to what we would expect from the picture put forward by SHS where once the overall \dot{M} starts declining, the corona responds faster and drains out sooner than compared to the disk. Thus the SHS model predicts that the powerlaw normalization will fall rather than the disk. Therefore while our data disagree with the particular mechanism discussed by SHS, they provide strong confirmation of the general idea that \ddot{M} , as well as \dot{M} , is an important factor

in governing state transitions.

The now well established fact that the hard to soft state transition occurs at a higher luminosity than that of soft to hard transition rules out one flow propeller models of accretion for Aql X-1. As discussed by Maccarone & Coppi (2003), the strong ADAF is also not tenable. The occurrence of this hysteresis phenomenon for all the recent outbursts of Aql X-1 further demonstrates that mass accretion rate is not the only factor in state transition in NS/BH systems.

From a compilation of RXTE data of several transient atoll sources, Gierliński & Done (2002) and Muno et al. (2002) have shown that the atolls form a “Z” shaped track in the color-color diagram, similar to Z sources. They conclude that both atolls and Z sources move along their tracks on the color-color plane and do not jump between the tracks. For the source 4U 1705-44 Gierliński & Done (2002) analysed the source movement with time and confirmed that the motion in the diagram goes along the track and they did not find any jump between the branches. Excellent coverage of the 2000 outburst of Aql X-1 allowed us to track its time evolution on the color-color plane quite closely. We found that although the overall time evolution does form a Z shape, the source jumps from the middle branch to the lower right instead of smoothly following a Z (Fig. 4). Thus the usual curve length parameter S does not describe the time evolution of the source for the outburst described here.

Interestingly, all the kHz QPOs seen in the data for this outburst were observed when the source was in the transitional soft state, in particular, once the 6.4-9.7 keV flux falls below ~ 50 counts/sec/PCU (Fig. 3). The kHz QPOs observed by Zhang et al. (1998) during the 1997 outburst of Aql X-1 also were seen during the declining phase, when the luminosity was considerably smaller than the peak value. In contrast Cui et al. (1998) reported kHz QPOs during the rising phase of the outburst of 1998. This might suggest that the TSS does occur in the rise, but has been missed because the rise is so much faster than the decline. But in all these 3 outbursts, kHz QPOs were observed during intermediate luminosity and never during very high or very low luminosity. Even the high frequency QPOs observed by Remillard et al. (2002) for black hole systems occur when the source is in a transitional state where the spectra is neither entirely dominated by the soft photons nor dominated by entirely hard photons.

If these QPOs are blobs of matter in Keplerian orbit around the compact object, then their radial distance (in km, given by r_{km}) from the compact star is $r_{km} \approx 15(\frac{m}{\nu_{qpo;kHz}})^{2/3}$, where m is the mass of the accretor in solar units and $\nu_{qpo;kHz}$ is the observed QPO frequency in kiloHertz. In this model the highest QPO frequency during the outburst observed around ~ 870 Hz puts the minimum radius of the QPOs between 17.5 and 23.7 km depending on the

neutron star mass (assumed to be between $1.2M_{\odot}$ and $3M_{\odot}$). According to the Keplerian orbit model of QPO origin, an increase in inferred mass accretion rate pushes the inner edge of the accretion disk inwards and therefore predicts QPO frequency to increase with \dot{M} and saturate beyond certain \dot{M} . In Fig. 11 we may see this saturation beyond ~ 400 counts/sec/PCU. However the fact that there are no QPOs when the source is either very faint or very bright supports the hypothesis put forward by Cui (2000) that the root of these kHz QPO lie in disk-magnetosphere interaction. The existence of a higher luminosity barrier can be regarded as an evidence for the presence of an innermost stable orbit.

DM would like to thank Tom Maccarone and Aya Kubota for their help with software. It is a pleasure to acknowledge the help of Paolo Coppi for many informative discussions and useful comments. This work was supported by National Science Foundation grant AST 00-98421 and NASA ADP grant NAG5-13336.

REFERENCES

Bailyn, C. D., Depoy, D., Agostinho, R., Mendez, R., Espinoza, J., & Gonzalez, D. 1999, BAAS, 31, 1502

Bradt, H. V., Rothschild, R. E., & Swank, J. H. 1993, A&AS, 97, 355

Belloni, T. & Hasinger, G. 1990, A&A, 227, L33

Belloni, T., Psaltis, D., & van der Klis, M. 2002, ApJ, 572, 392

Callanan, P. J., Filippenko, A. V., & Garcia, M. R. 1999, IAU Circ., 7086, 3

Campana, S. & Stella, L. 2000, ApJ, 541, 849

Chen, W., Shrader, C. R., & Livio, M. 1997, ApJ, 491, 312

Chevalier, C., Ilovaisky, S. A., Leisy, P., & Patat, F. 1999, A&A, 347, L51

Cui, W. 2000, ApJ, 534, L31

Cui, W., Zhang, S. N., Focke, W., & Swank, J. H. 1997, ApJ, 484, 383

Cui, W., Barret, D., Zhang, S. N., Chen, W., Boirin, L., & Swank, J. 1998, ApJ, 502, L49

Czerny, M., Czerny, B., & Grindlay, J. E. 1987, ApJ, 312, 122

Dubus, G., Hameury, J.-M., & Lasota, J.-P. 2001, A&A, 373, 251

Gierliński, M. & Done, C. 2002, MNRAS, 331, L47

Giles, A. B., Swank, J. H., Jahoda, K., Zhang, W., Strohmayer, T., Stark, M. J., & Morgan, E. H. 1996, ApJ, 469, L25

Hasinger, G. & van der Klis, M. 1989, A&A, 225, 79

Homan, J., Wijnands, R., van der Klis, M., Belloni, T., van Paradijs, J., Klein-Wolt, M., Fender, R., & Méndez, M. 2001, ApJS, 132, 377

Jahoda, K., Swank, J. H., Giles, A. B., Stark, M. J., Strohmayer, T., Zhang, W., & Morgan, E. H. 1996, Proc. SPIE, 2808, 59

Jain, R. K. 2001, Ph.D. Thesis, Yale University

Kaaret, P., Yu, W., Ford, E. C., & Zhang, S. N. 1998, ApJ, 497, L93

King, A. R. & Ritter, H. 1998, MNRAS, 293, L42

Koyama, K. et al. 1981, ApJ, 247, L27

Leahy, D. A., Darbro, W., Elsner, R. F., Weisskopf, M. C., Kahn, S., Sutherland, P. G., & Grindlay, J. E. 1983, ApJ, 266, 160

Levine, A. M., Bradt, H., Cui, W., Jernigan, J. G., Morgan, E. H., Remillard, R., Shirey, R. E., & Smith, D. A. 1996, ApJ, 469, L33

Maccarone, T. J. & Coppi, P. S. 2003, MNRAS, 338, 189

Markoff, S., Falcke, H., & Fender, R. 2001, A&A, 372, L25

Méndez, M., van der Klis, M., Ford, E. C., Wijnands, R., & van Paradijs, J. 1999, ApJ, 511, L49

Mitsuda, K. et al. 1984, PASJ, 36, 741

Miyamoto, S., Kitamoto, S., Hayashida, K., & Egoshi, W. 1995, ApJ, 442, L13

Morrison, R. & McCammon, D. 1983, ApJ, 270, 119

Muno, M. P., Remillard, R. A., & Chakrabarty, D. 2002, ApJ, 568, L35

Nowak, M. A. 1995, PASP, 107, 1207

Nowak, M. A. 2002 (astro-ph/0207624)

Orosz, J. A., Remillard, R. A., Bailyn, C. D., & McClintock, J. E. 1997, *ApJ*, 478, L83

Reig, P., Méndez, M., van der Klis, M., & Ford, E. C. 2000, *ApJ*, 530, 916

Remillard, R. A., Muno, M. P., McClintock, J. E., & Orosz, J. A. 2002, *ApJ*, 580, 1030

Rutledge, R. E., Bildsten, L., Brown, E. F., Pavlov, G. G., & Zavlin, V. E. 1999, *ApJ*, 514, 945

Rutledge, R. E., Bildsten, L., Brown, E. F., Pavlov, G. G., & Zavlin, V. E. 2000, *ApJ*, 529, 985

Rutledge, R. E., Bildsten, L., Brown, E. F., Pavlov, G. G., & Zavlin, V. E. 2001, *ApJ*, 559, 1054

Shakura, N. I. & Sunyaev, R. A. 1973, *A&A*, 24, 337

Šimon, V. 2002, *A&A*, 381, 151

Smith, D. M., Heindl, W. A., & Swank, J. H. 2002, *ApJ*, 569, 362 (SHS)

Sunyaev, R. A. & Titarchuk, L. G. 1980, *A&A*, 86, 121

van der Klis, M. 1995, in X-ray Binaries, ed. W. W. G. Lewin, J. van Paradijs & E. P. J. van den Heuvel (Cambridge: Cambridge Univ. Press) 252

van der Klis, M. 2000, *ARA&A*, 38, 717

van der Klis, M. 2001, *ApJ*, 561, 943

Welsh, W. F., Robinson, E. L., & Young, P. 2000, *AJ*, 120, 943

Yu, W., Klein-Wolt, M., Fender, R., & van der Klis, M. 2003, *ApJ*, 589, L33

Zhang, W., Jahoda, K., Kelley, R. L., Strohmayer, T. E., Swank, J. H., & Zhang, S. N. 1998, *ApJ*, 495, L9

Zhang, S. N., Yu, W., & Zhang, W. 1998, *ApJ*, 494, L71

Table 1. Results of Spectral Deconvolution

Srl. No.	ObsID	Time (MJD)*	Exposure (ks) [†]	T_{in} (keV)	Photon Index	$(\chi^2/dof)^{\ddagger}$
1	50049-01-03-00	51811.26	5.59	0.57 ± 0.08	1.65 ± 0.06	0.59
2	50049-01-03-01	51812.31	3.50	0.60 ± 0.15	1.73 ± 0.03	0.66
3	50049-01-03-02	51813.25	5.34	0.86 ± 0.19	1.67 ± 0.08	0.41
4	50049-01-04-00	51816.43	3.41	2.40 ± 0.30	1.56 ± 0.07	0.41
5	50049-01-04-01	51817.77	2.06	3.37 ± 0.50	1.55 ± 0.04	0.35
6	50049-01-04-02	51818.76	3.48	3.60 ± 0.50	1.60 ± 0.04	0.58
7	50049-01-04-03	51820.48	3.43	3.90 ± 0.40	1.50 ± 0.06	0.55
8	50049-01-04-04	51822.74	3.37	2.26 ± 0.05	2.96 ± 0.10	0.61
9	50049-01-05-00	51823.73	3.25	2.37 ± 0.04	3.07 ± 0.13	0.78
10	50049-01-05-01	51824.73	3.01	2.30 ± 0.09	3.05 ± 0.17	0.46
11	50049-01-05-02	51825.73	3.41	2.25 ± 0.09	3.22 ± 0.14	0.42
12	50049-02-01-00	51826.49	9.21	2.49 ± 0.04	3.50 ± 0.30	0.25
13	50049-02-02-00	51828.53	13.23	2.29 ± 0.03	3.29 ± 0.08	0.54
14	50049-02-03-01	51831.17	2.86	2.42 ± 0.03	3.26 ± 0.11	0.44
15	50049-02-03-00	51833.42	2.77	2.23 ± 0.08	3.23 ± 0.10	0.31
16	50049-02-04-00	51834.29	14.97	2.49 ± 0.08	3.40 ± 0.30	0.50
17	50049-02-03-02	51835.15	2.91	2.34 ± 0.03	3.27 ± 0.08	0.33
18	50049-02-05-00	51835.45	9.39	2.47 ± 0.03	3.27 ± 0.18	0.32
19	50049-02-06-00	51836.48	3.42	2.25 ± 0.06	2.96 ± 0.17	1.13
20	50049-02-06-01	51836.56	1.87	2.23 ± 0.09	2.90 ± 0.42	0.88
21	50049-02-06-02	51836.63	1.34	2.31 ± 0.03	3.25 ± 0.11	0.64
22	50049-02-07-00	51837.28	3.50	2.44 ± 0.08	3.07 ± 0.17	0.32
23	50049-02-07-01	51838.55	1.80	2.34 ± 0.05	3.46 ± 0.28	0.74
24	50049-02-07-02	51839.13	2.78	2.36 ± 0.06	3.81 ± 0.83	0.48
25	50049-02-07-03	51841.40	2.82	2.33 ± 0.03	3.17 ± 0.08	0.43
26	50049-02-07-04	51843.39	2.91	2.36 ± 0.06	2.94 ± 0.13	0.67
27	50049-02-08-00	51844.12	14.94	2.36 ± 0.08	3.02 ± 0.11	0.35
28	50049-02-08-01	51845.11	2.35	2.45 ± 0.09	3.29 ± 0.26	0.65
29	50049-02-08-03	51846.18	3.46	2.30 ± 0.06	3.25 ± 0.12	0.33
30	50049-02-09-00G	51847.01	9.20	2.31 ± 0.03	3.32 ± 0.08	0.32
31	50049-02-10-03	51849.36	1.57	2.28 ± 0.03	3.41 ± 0.11	0.41
32	50049-02-10-02	51849.43	1.79	2.28 ± 0.03	3.46 ± 0.12	1.01
33	50049-02-10-01	51849.50	2.13	2.35 ± 0.10	3.16 ± 0.16	0.30
34	50049-02-10-00	51850.09	14.89	2.33 ± 0.06	3.22 ± 0.11	0.32
35	50049-02-10-05	51850.86	9.13	2.37 ± 0.03	3.45 ± 0.11	0.73
36	50049-02-11-00	51851.28	14.53	2.28 ± 0.09	3.26 ± 0.14	0.45
37	50049-02-11-01	51852.56	2.08	2.27 ± 0.05	3.13 ± 0.19	0.65

Table 1—Continued

Srl. No.	ObsID	Time (MJD)*	Exposure (ks) [†]	T_{in} (keV)	Photon Index	$(\chi^2/dof)^{\ddagger}$
38	50049-02-11-02	51852.62	1.02	2.35 ± 0.13	3.07 ± 0.28	0.57
39	50049-02-12-01	51853.55	2.06	2.27 ± 0.05	3.33 ± 0.16	0.70
40	50049-02-12-00	51854.27	15.00	2.31 ± 0.09	3.26 ± 0.10	0.37
41	50049-02-13-00	51855.27	3.16	2.33 ± 0.08	3.46 ± 0.12	0.67
42	50049-02-13-01	51856.17	9.21	2.36 ± 0.03	3.23 ± 0.08	0.55
43	50049-02-14-00	51856.97	18.79	2.36 ± 0.03	3.42 ± 0.07	0.48
44	50049-02-15-00	51859.25	15.04	2.36 ± 0.09	3.36 ± 0.13	0.55
45	50049-02-15-01	51860.18	3.51	2.29 ± 0.04	3.29 ± 0.10	0.49
46	50049-02-15-08	51860.52	1.86	2.33 ± 0.05	3.45 ± 0.14	0.42
47	50049-02-15-02	51861.12	13.74	2.32 ± 0.10	3.20 ± 0.08	0.40
48	50049-02-15-03	51861.88	7.87	2.38 ± 0.07	3.28 ± 0.09	0.56
49	50049-02-15-04	51862.08	7.74	2.31 ± 0.06	3.40 ± 0.08	1.06
50	50049-02-15-05	51863.24	14.96	2.43 ± 0.09	2.87 ± 0.06	0.85
51	50049-02-15-06	51864.17	2.05	2.44 ± 0.08	3.25 ± 0.12	0.99
52	50049-02-15-07	51864.24	1.52	2.57 ± 0.10	3.13 ± 0.14	0.75
53	50049-03-01-00	51865.24	1.67	3.74 ± 0.64	2.24 ± 0.10	0.60
54	50049-03-02-01	51866.89	0.85	0.67 ± 0.27	1.75 ± 0.19	0.98
55	50049-03-02-00	51866.95	2.44	0.86 ± 0.16	1.69 ± 0.15	0.58
56	50049-03-03-00	51868.20	1.93	0.65 ± 0.10	1.59 ± 0.06	0.79
57	50049-03-04-00	51869.45	7.29	0.47 ± 0.07	1.60 ± 0.05	0.83
58	50049-03-05-00	51870.30	8.66	0.47 ± 0.09	1.41 ± 0.06	0.78
59	50049-03-06-00	51871.21	1.83	0.35 ± 0.10	1.11 ± 0.24	0.75
60	50049-03-07-00	51872.13	3.33	0.45 ± 0.10	0.82 ± 0.11	0.83
61	50049-03-08-00	51874.29	6.39	0.34 ± 0.10	0.90 ± 0.18	0.55
62	50049-03-09-00	51876.31	3.43	0.38 ± 0.09	0.62 ± 0.16	0.70
63	50049-03-10-00	51878.14	8.02	0.34 ± 0.09	0.67 ± 0.16	0.89

*Observation starting time

[†]Total exposure time before screening for good time intervals

[‡] $dof = 31$

Table 2. PDS Parameters for hard state dwells in rising phase

Time(MJD)	f_{br} (Hz)	α_1	α_2	f_{qpo} (Hz)	FWHM(Hz)	rms_{qpo} (%)
51813.3	$0.26^{+0.21}_{-0.08}$	$-0.7^{+0.2}_{-0.2}$	$-1.08^{+0.04}_{-0.06}$
51816.5	$0.34^{+0.22}_{-0.11}$	$-0.4^{+0.6}_{-0.3}$	$-0.96^{+0.03}_{-0.03}$	$1.8^{+0.2}_{-0.2}$	$2.4^{+0.5}_{-0.4}$	$10.6^{+2.0}_{-1.8}$
51817.8	$0.38^{+0.06}_{-0.06}$	$-0.1^{+0.3}_{-0.2}$	$-0.96^{+0.02}_{-0.02}$	$2.3^{+0.2}_{-0.2}$	$3.2^{+0.5}_{-0.4}$	$12.1^{+1.5}_{-1.4}$
51818.8	$0.42^{+0.08}_{-0.12}$	$-0.3^{+0.2}_{-0.2}$	$-0.96^{+0.02}_{-0.02}$	$2.5^{+0.2}_{-0.2}$	$3.8^{+0.4}_{-0.4}$	$13.0^{+1.1}_{-1.2}$
51820.5	$0.86^{+0.08}_{-0.12}$	$-0.1^{+0.1}_{-0.1}$	$-1.10^{+0.04}_{-0.04}$	$5.4^{+0.2}_{-0.3}$	$6.4^{+0.8}_{-0.6}$	$13.1^{+1.2}_{-1.0}$

Table 3. Observed kHz QPOs

Time(Days)	Frequency (Hz)	FWHM (Hz)	Fractional RMS (%)
51855.29	$833.7^{+1.3}_{-1.2}$	$12.8^{+3.9}_{-2.9}$	$4.4^{+1.2}_{-0.9}$
51861.87	$869.9^{+0.5}_{-0.4}$	$07.0^{+2.0}_{-2.1}$	$5.5^{+1.7}_{-1.3}$
51861.92	$832.5^{+1.5}_{-1.3}$	$19.4^{+3.6}_{-2.9}$	$6.8^{+1.0}_{-0.9}$
51862.07	$812.2^{+1.2}_{-1.0}$	$09.8^{+2.0}_{-1.4}$	$6.6^{+1.2}_{-0.8}$
51862.12	$754.6^{+1.2}_{-1.1}$	$13.4^{+3.2}_{-2.7}$	$6.6^{+1.1}_{-1.3}$
51863.19	$636.5^{+1.3}_{-1.5}$	$16.2^{+4.9}_{-4.1}$	$6.3^{+1.6}_{-1.3}$
51863.25	$646.2^{+2.1}_{-2.2}$	$22.0^{+6.1}_{-4.5}$	$6.6^{+1.2}_{-1.3}$
51864.20	$716.3^{+0.6}_{-0.5}$	$07.3^{+1.3}_{-1.2}$	$7.5^{+1.1}_{-1.1}$
51864.27	$702.3^{+2.5}_{-2.1}$	$09.6^{+5.1}_{-3.9}$	$5.8^{+2.6}_{-2.3}$

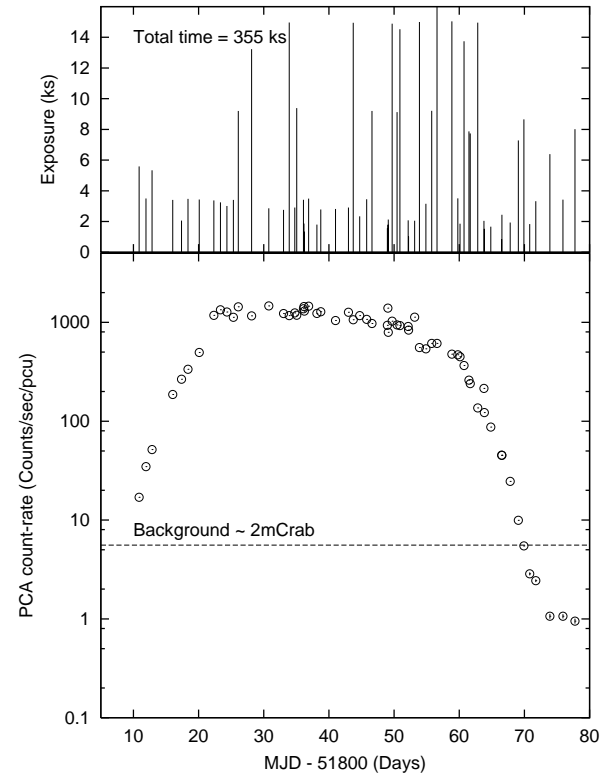


Fig. 1.— RXTE data from 2000 outburst of Aql X-1. (Top) Exposure times for the 63 PCA dwells. (Bottom) Full-range (≈ 2 - 60 keV) background subtracted PCA light curve.

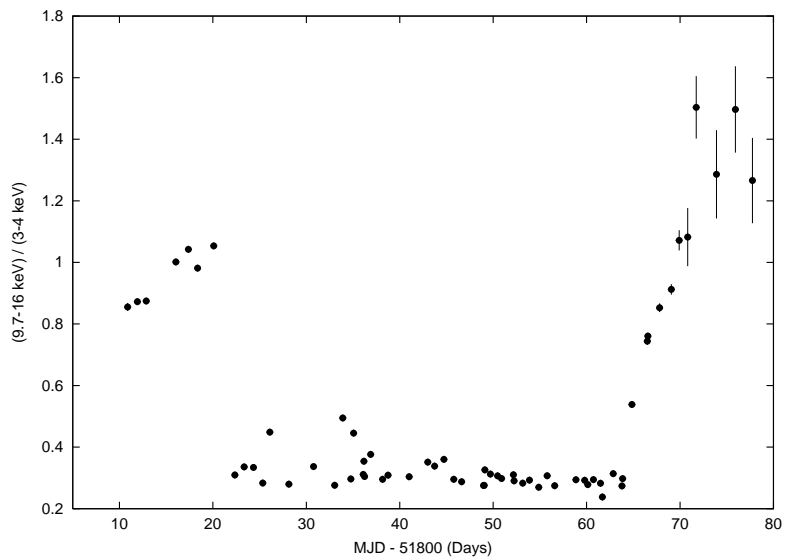


Fig. 2.— Variation of hardness, defined as counts in 9.7-16 keV range divided by counts in 3-4 keV range, with time for the 2000 outburst of Aql X-1.

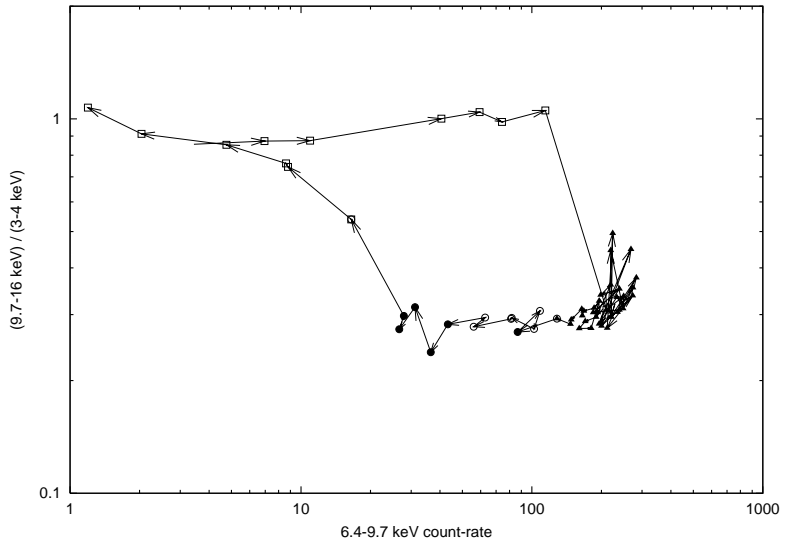


Fig. 3.— Evolution of Aql X-1 on X-ray color luminosity diagram. The arrows point in the direction of advancing time. Observations corresponding to the source being in the *hard state* are shown as open squares, the *canonical soft state* is shown by filled triangles and *transitional soft state* is shown by circles. The errorbars become larger towards the left (because very few photons are detected during the very early as well as very late phase of the outburst). However for the range of hardness and intensity plotted, the errorbars are smaller than the symbol size and hence not plotted. The dwells for which kHz QPOs were detected are indicated by filled circles.

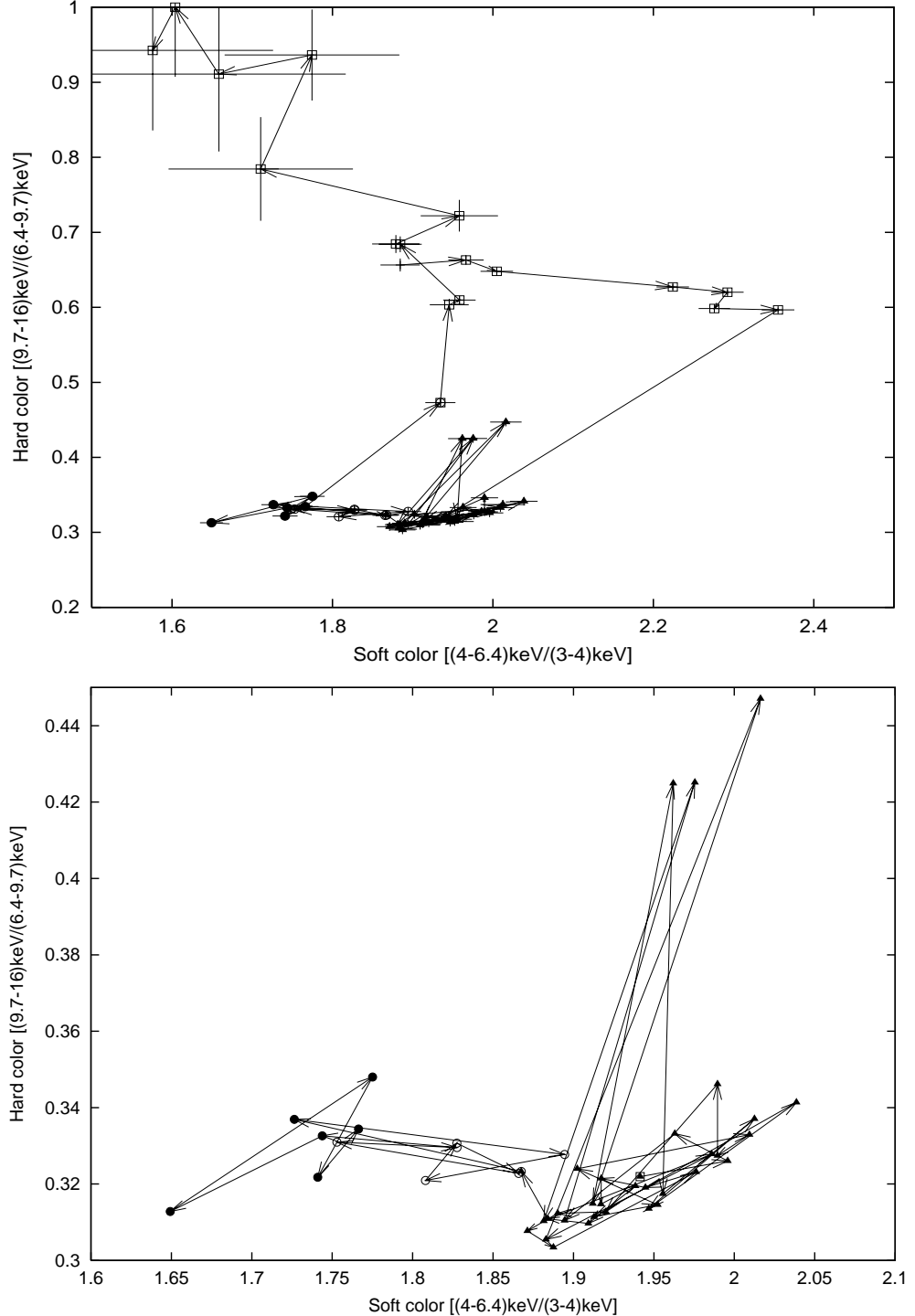


Fig. 4.— (Top) Evolution on the Color-color plane during the entire outburst. The symbols have the same meaning as in Fig. 3. (Bottom) Blow-up of the region corresponding to the soft state. The errorbars have not been plotted in the bottom plot to avoid confusion.

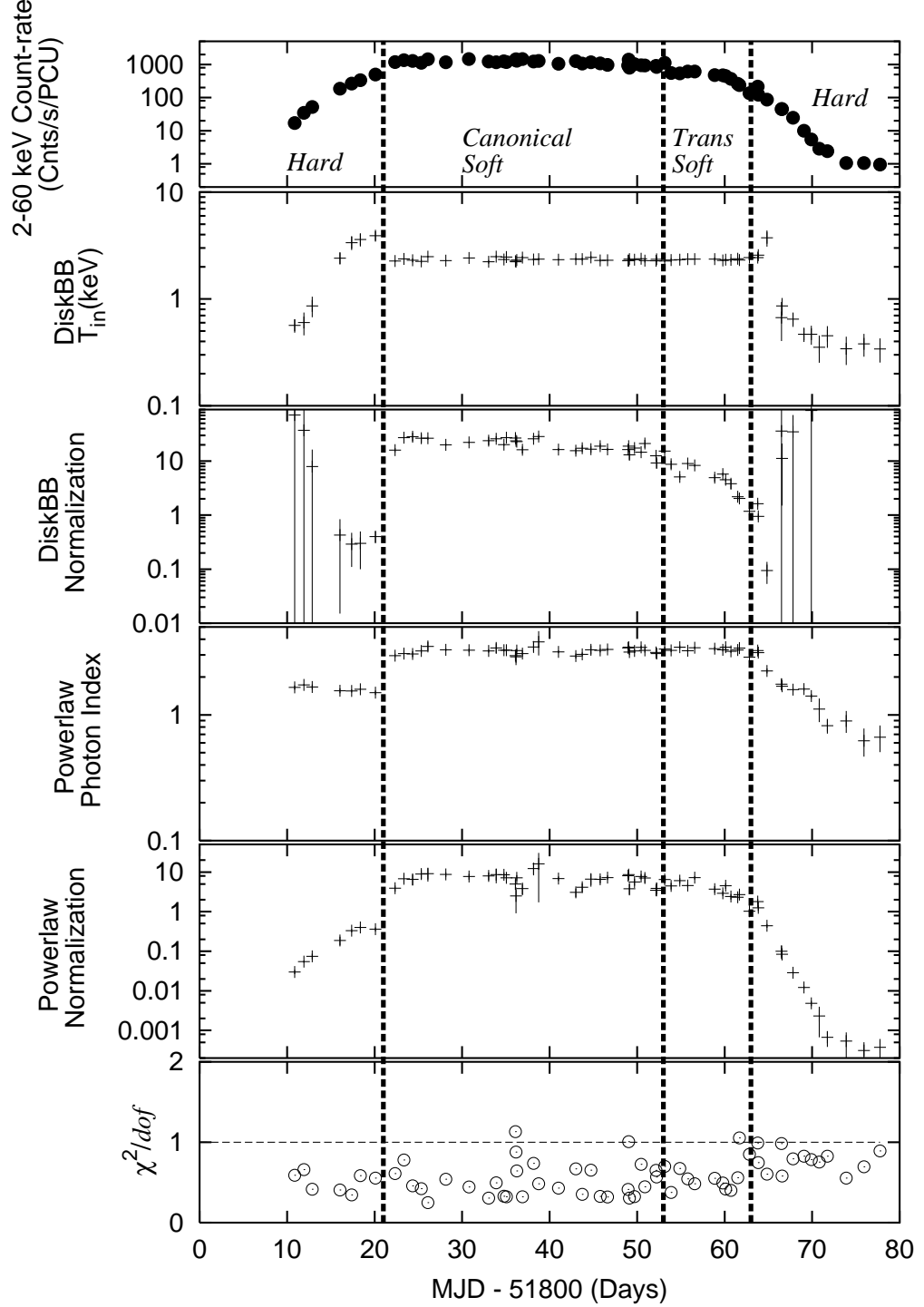


Fig. 5.— Spectral deconvolution, evolution of the spectral fit parameters with time during the outburst of Aql X-1. The different spectral states as defined from the color-color plot (Fig 4) are separated by the thick dashed lines.

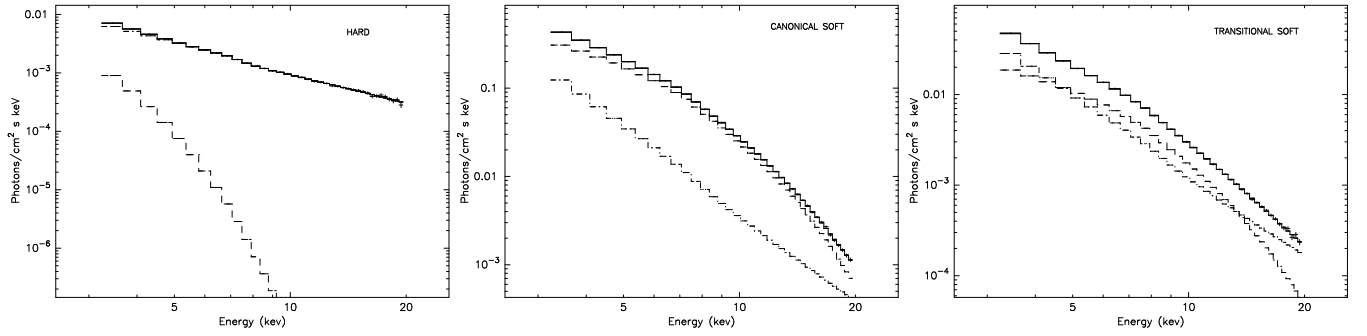


Fig. 6.— Sample unfolded spectra during the various states. Left: Hard state spectrum for the dwell on MJD 51812.31. Middle: Canonical soft state as seen on MJD 51836.63. Right: Transitional soft state on MJD 51863.24. The dashed histogram is the fitted disk blackbody, dash-dotted histogram is the powerlaw, solid histogram is the overall fit and the crosses (only visible near higher end of the spectra) are the data points. Note that the primary difference between the canonical soft state and the transitional soft state is the lower relative normalization of the disk component in the transitional soft state.

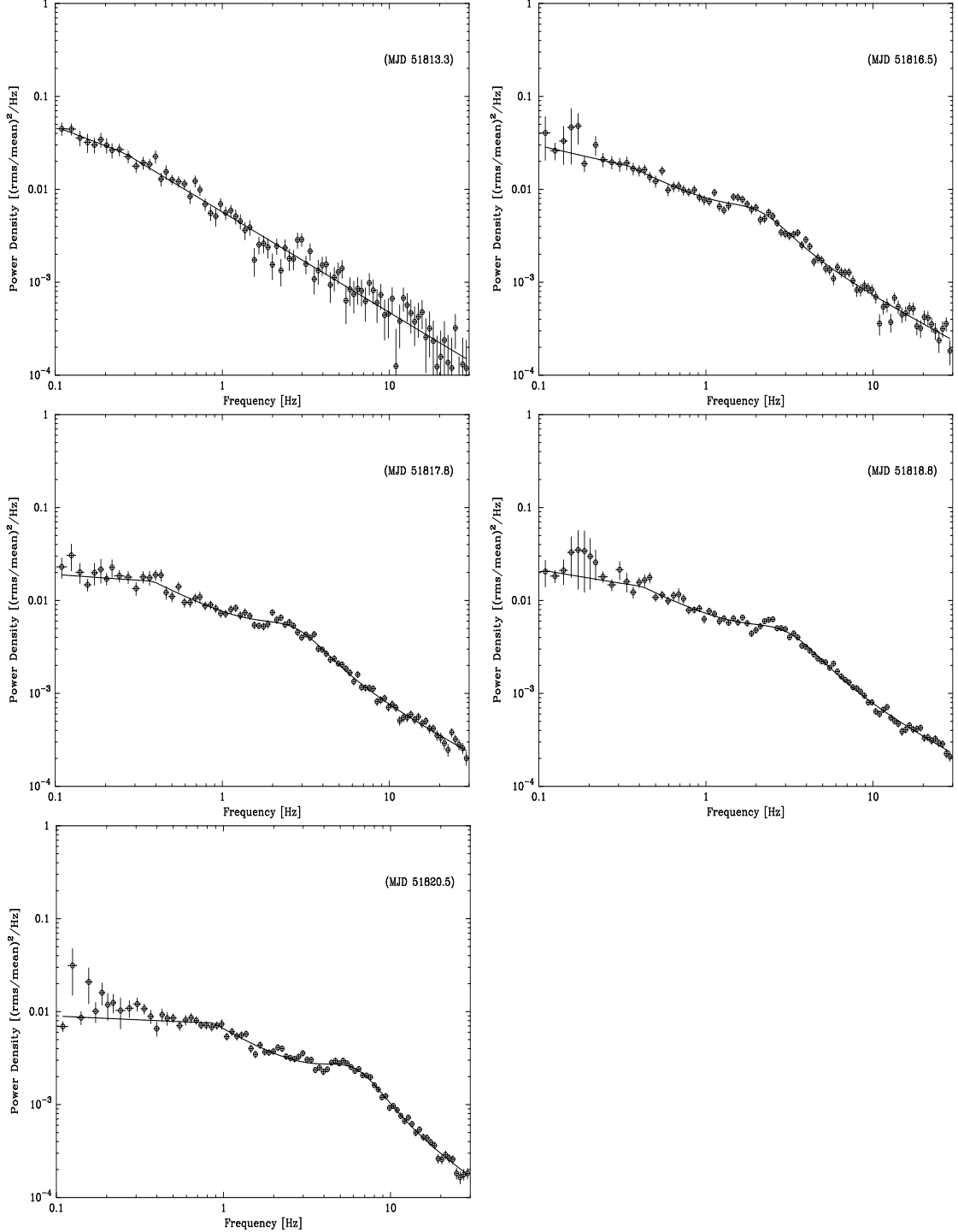


Fig. 7.— Low frequency PDS during the rising phase. The time of observation is shown in top right corner for each plot. The ordinate represents the Poisson noise subtracted PDS renormalized by the mean count rate, plotted against temporal frequency along the abscissae.

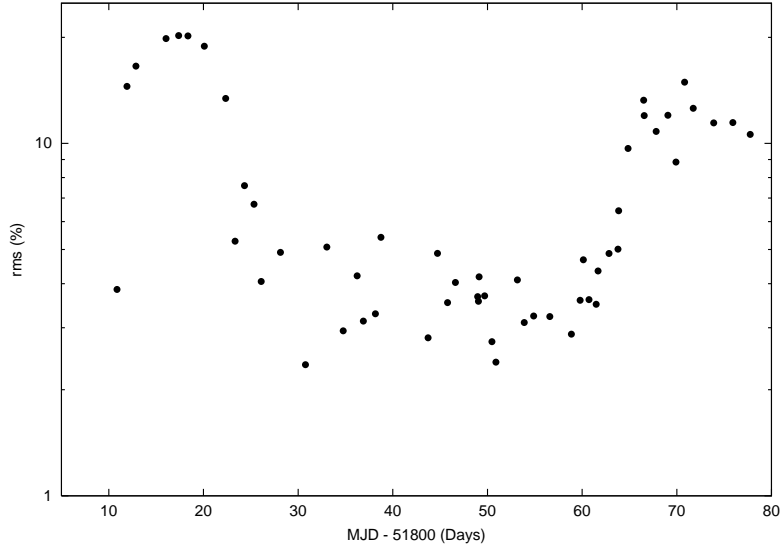


Fig. 8.— Evolution of time-variability. The total rms variability in the Fourier power spectrum between 0.1-30 Hz is plotted against time. Each dwell is one point in the diagram.

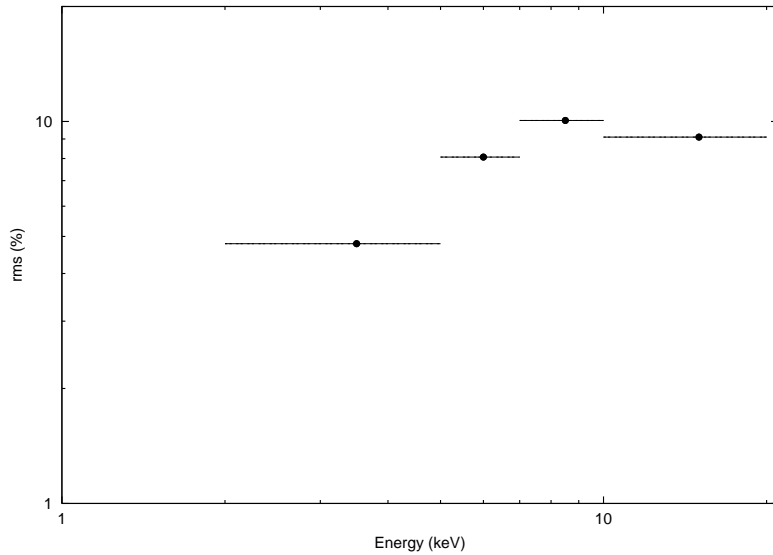


Fig. 9.— Rms energy spectra for a soft state dwell ($t=51863.78$ day). Percentage rms variability for the energy ranges 2-5, 5-7, 7-10 and 10-20 keV are plotted.

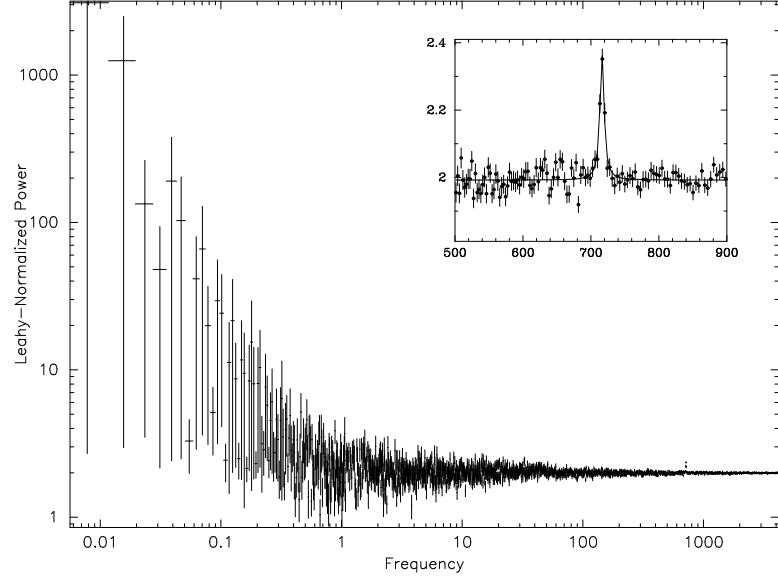


Fig. 10.— A sample time-averaged PDS from 0.01 Hz to 4 kHz for the dwell starting MJD 51864.17. The region around the QPO is blown up and shown in the inset. The spectrum above 100 Hz is essentially dominated by Poisson counting statistics.

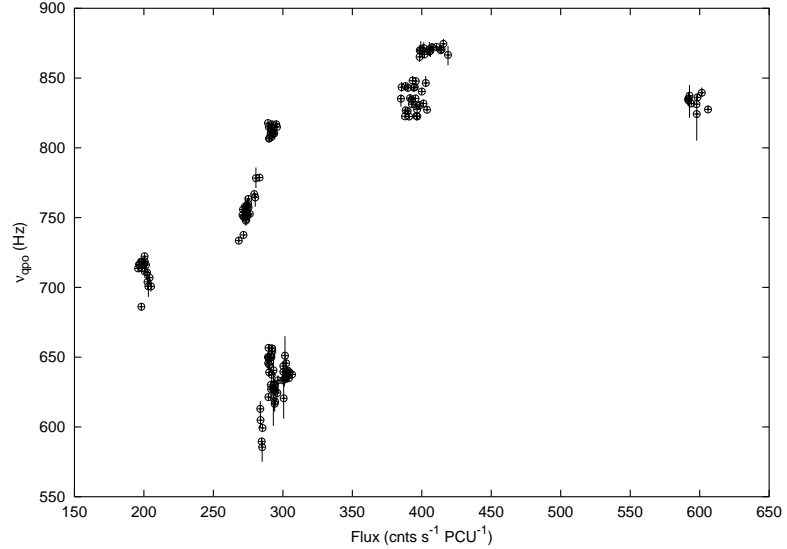


Fig. 11.— Observed kHz QPO frequency vs. count rate showing the “parallel tracks” as they occur during the 2000 outburst of Aql X-1.